Numerical Investigation of Simultaneous Refractive index Sensor using 1D multichannel photonic crystal device

A. Bouzidi
Universite Mohammed V de Rabat Faculte des Sciences
D. Bria
Universite Mohammed V de Rabat Faculte des Sciences
Hala J. El-Khozondar
Gaza University
D Vigneswaran
Sri Krishna Engineering College
Shobhit K. Patel
Marwadi University
N.R. Ramanujam
KLN College of Engineering
Kawsar Ahmed (kawsar.ict@mbstu.ac.bd)
Mawlana Bhashani Science and Technology University https://orcid.org/0000-0002-4034-9819

Research

Keywords: 1D Photonic Crystal, Multichannel, Defects, Sensitivity, Optical Sensor

Posted Date: April 27th, 2020

DOI: https://doi.org/10.21203/rs.3.rs-23481/v1

Abstract

We present a multichannel sensor for the simultaneous monitoring of three different samples. established from a one-dimensional photonic crystal, this device is formed by an alternating layer of silicon dioxide (SiO2) and titanium dioxide (TiO2) with three defect layers containing the samples to be monitored. Numerical studies claim that three transmission peaks appear in the bandgap, these transmission peaks are caused by the three samples infiltrated in the defect layers. In real-time detection purposes, it is possible to exploit these transmission peaks. In addition, peak frequencies have the advantage of being susceptible to sample concentrations. With this photonic structure, a sensitivity of 800 nm per unit of refractive index (RIU) is reached.

1. Introduction

Sensor is a device which senses the physical, biological and chemical changes in parameters such as refractive index [1–4], temperature [5], pressure [6], pH [7], gas [8], magnetic fluid [9] and so on. Sensors based on optics have a lot of attention in detecting the small changes in temperature, pressure, chemical composition etc., due to their high sensitivity [10]. The designs of optical devices based on the periodic structures have been developed recently. Photonic Crystal (PC) is a periodic structure with different dielectric constant which controls the light guiding properties and the existence of the photonic band gap (PBG) is an interesting property of PC. It prohibits the propagation of electromagnetic waves inside the PC. It can control the guiding of photons in PC. It can also control the localization of light and spontaneous emission. The periodic structure of PC is broken entirely by introducing the defects which allows controlling and manipulating the light. PC based optical devices such as filters, logic gates, sensors [11] were reported earlier.

The various devices such as sensors, splitters and multiplexers based on the PC material are designed and fabricated in recent years. These sensors are also emerging in the field of healthcare, defence, security, aerospace, environment and food quality control [12, 13] based on the principle of photonics. The applications of PC sensors are also extended to identify DNA, protein cell, bacteria [14] and are highly efficient. Different blood components such as glucose and haemoglobin are detected and simulated in a PC ring resonator and the effect of parameters are investigated. These blood constituents are analysed by using the photonic sensing technology [15]. The propagation of electromagnetic waves is affected while passing the PC structure with this blood components, the permittivity of the biological molecules is greater than those of air and water.

The functional materials of magnetic fluids have been investigated due to their special magnetic properties based on the combination of solid magnetic particles and the fluidity of the liquid [16]. By adjusting the strength of the critical magnetic field [17], the refractive index of magnetic fluids can be changed. A sensor based on magnetic field and temperature in a magnetic field which is infiltrated into the PC cavity is investigated by Zhao et al. [18]. In refractive index mechanism, the characteristics of the transmission spectra will be changed due to their change in the refractive index of the biological molecule

which is bind to the active sensing surface. The detection of analytes such as blood glucose [19], cancer cell [20], and blood plasma [21] are reported earlier by PC cavity technique. The sensor is able to sense three different analytes with their refractive indices simultaneously which have some cavities and are investigated with three cavities by author [22]. In the present work, three different analytes such as haemoglobin, urine and magnetic fluid are sensed with multiple cavities simultaneously by using the PC device.

2. Methods

The aim of the research is to design a multichannel sensor based model which can monitor different samples simultaneously. The geometric model is shown in Fig. 1. It is of the form AB^N *Def1* BA^M *Def2* AB^M *Def3* BA^N, where M and N denote the numbers of AB bilayers placed on either side of the defect layer, Def I (I = 1, 2 or 3). A photonic structure cell is formed by two dielectric layers (layer A and layer B). In the xy plane are located the layers of the PC, the z axis is perpendicular to the interfaces of the layers. We assume that the layers are infinite along the x and y directions, while the photonic structure is finite along the z direction (Fig. 1). The width of the layers A, B and Def are d_A, d_B and d_{Def}, respectively. $d = d_A + d_B$ is the period of the structure. The materials making up the layers of the photonic structure are considered to be homogeneous and not magnetic. Layers A and B are defined by the refractive index n_A and n_B respectively.

Several techniques are used in the study of the propagation of electromagnetic waves in periodic structures, among these methods there is the transfer matrix method and the Green function method. These two methods allow us to determine the dispersion relation, the transmission and reflection coefficients [23]. Velasco et al. and El Boudouti et al. have established a remarkable relationship between transfer matrices and Green's functions. This combination allows the study of the physical properties of any composite system. In this paper, we use the interface response theory of continuous media, a simple presentation of the Green function [24–26]. This technique is the most suitable for the treatment of composite systems containing several interfaces [27, 28].

3. Results And Discussion

We consider a one-dimensional photonic structure of finite size AB^N *Def1* BA^M *Def2* AB^M *Def3* BA^N, as depicted in Fig. 1. The analytes to be sensed are introduced into the cavities (*Def1, Def2, and Def3)*. A spectrometer detects the light emitted by the source after its transmission from the photonic crystal.

Fig. 2 shows the one-dimensional structure which is used to calculate the transmission spectra. The periodic layers from each part of the three defects layers, Def1, Def2, and Def3, are made of two materials, A and B. It is assumed that the layers A of thickness d_A to be silicon dioxide SiO_2. The layers B of thickness d_B are titanium dioxide TiO_2. The period of perfect structure is $d=d_A+d_B$. The choice of these dielectrics is justified by the very wide use of these two materials SiO2 and TiO2 [29] as substrates for

photonic structures of detection. the PC is enveloped by air. The three defects layers, Def1, Def2, and Def3, will be filled by three different analytes. In our study, we will change the lengths of the defect layers.

We consider a normal incidence of light on the left surface of the PC. Incident light is linearly polarized: TE-polarizations.

In order to use the configuration of Fig. 1 for simultaneous detection of three analyte samples, the usual approach is to define special characteristics like transmission peaks in the transmission spectrum. We will show that, at normal incidence, the resonances corresponding to the three defects can occur in the transmission spectrum only with a good choice of the thickness of these three layers defects. Then we discuss the occurrence of resonances modes according to thickness d_{Def}, and after we study the change of the refractive index, with the aim of having the three defects modes corresponding to the three defect layers inside the photonic structure band gap.

In this section, we analyze numerically the transmission spectrum as a function of the defect layers thickness, and as a function of the sample concentrations. In this article, we limit our study to the first PBG of spectra. For the numerical calculations we choose the following parameters of the PC: the PC's period d = 1360 nm, and the dielectric layer thicknesses d_A=952 nm and d_B=408 nm. The thickness of the dielectric defect layers is equal to d_{Def} = 1713.6 nm. The refractive indices for the photonic crystal constituents are equal to n_A=1.45 (for SiO_2), n_B=2.46 (for TiO_2).

We display the transmittances according to the frequency for a regular PC (black lines) and a defective PC (blue lines) in Fig. 3. we assume that the incidence of the electromagnetic wave towards the photonic structure is normal. It is shown that for these three thickness values of the defect layers, the defect modes occur inside the transmission spectrum PBGs. From the study of Fig. 3, it can be noted that when d_{Def} = 272 nm, two defect modes appear in the band gap (blue curves), localized at f = 5.8060 e^{+13}Hz, and f = 6.2847 e^{+13}Hz in the infrared (IR) regions, when d_{Def} = 843.2 nm, one defect mode appears in the band gap (blue curves), localized at f = 7.1384 e^{+13}Hz, and when d_{Def} = 1713.6 nm, three defect modes appear in the band gap (blue curves), localized at f = 5.9009 e^{+13}Hz, f = 6.4060 e^{+13}Hz, and f = 6.7402 e^{+13}Hz. These findings clearly show that the thickness of the defect layers changes the defect modes properties within the IR regions.

We deduced that the change of three layers of the perfect photonic crystal with other layers, induces the appearance of peaks inside the forbidden bands. Consequently, the choice of d_{Def} (or the ratio d_{Def} / d), is a determining indicator in the occurrence, the tunability, the sensibility and the controlling of the peaks within the forbidden band of the PC. It implies that, for detection purposes, the parameters of the photonic crystal should be well defined in order to have isolated peaks in the forbidden band. This is closely related to the optimization of an efficient sensor with high sensitivity and wide measurement spectrum.

In order to better understand the existence and the comportment of the defect modes as a function of d_{Def}, we studied the progress of the reduced frequencies of the transmission according to the length d_{Def}, in the PC with three defects. Figure 4 shows the results, the black dotted lines denote the maximum transmission. However, the primrose yellow zones represent the PBG. It can be seen that with this super lattice we have two band gaps, the first one is between 50 THz – 75 THz, and the second one is between 179 THz − 198 THz, branches appear automatically inside the band gap. the frequencies of these branches rely upon the length d_{Def}.

if we look at the first bandgap (50thz – 75thz), when 100 nm < d_{Def} <400 nm, two defects modes occur in the band gap, when 700 nm < d_{Def} <1100 nm, only one defect mode appear in the band gap, and when 1700nm < d_{Def} <2100 nm three defects modes appears in the band gap.As a summary, one can say that in order to bring up the three defect modes corresponding to the three defects introduced into the photonic structure, the value of the thickness of the defect layers must be between 1700 nm and 2100 nm to design a sensor, we must form a structure with which the transmission coefficient has well-defined characteristics as well as a very high sensitivity to infiltrating samples.

We introduce the defect layer1, defect layer2 and defect layer 3 to monitor the concentration of magnetic fluid, hemoglobin and salt in urine. We are varying the concentration of each sample and will analyse the behaviour of the defect modes corresponding to each defect layer.

We report the evolution of the transmission curves in Fig. 5. When the refractive index of the magnetic fluid which is infiltrated in the defect layer 1 is increased, we notice a displacement of the peak characterizing this defect layer towards the lowest frequencies; we also noticed that there is a reduction in the transmission of the defect peak. When we increase the refractive index of the hemoglobin in the defect layer 2, we notice a displacement of the peak characterizing this defect layer towards the lowest frequencies, so the transmission of the defect peak decreases when the refractive index increases. When we increase the refractive index of the urine which is infiltrated into the defect layer 3, we always notice a displacement of the peak characterizing this defect layer towards the lowest frequencies, but here the transmission of the defect peak increases with the increase in the refractive index. These results are summarized in Tables 1, 2, and 3 along with the quality factors of the defect peaks.

Table 1
Keeping defect 2 (hemoglobin), and defect 3 (urine) refractive indices constant and changing the refractive index of the defect 1 (magnetic fluid).

D_{Def}(nm)	Defects1 peak frequency	Q-factor	Oe	Refractive Index
1713.6 nm	5.9012 e^{+13}	3471	89.9	1.4635
	5.9006 e^{+13}	3105	120.3	1.4645
	5.9002 e^{+13}	2935	150.0	1.4654
	5.8997 e^{+13}	2783	180.4	1.4662

Table 2
Keeping defect 1 (magnetic fluid), and defect 3 (urine) refractive indices constant and changing the refractive index of the defect 2 (hemoglobin).

D_{Def}(nm)	Defects2 peak frequency	Q-factor	Concentration(g/l)	Refractive Index
1713.6 nm	6.4056 e^{+13}	2128	10	1.341299324
	6.4011 e^{+13}	2140	20	1.360719324
	6.3922 e^{+13}	2145	30	1.399559324
	6.3836 e^{+13}	2263	40	1.438399324

Table 3
Keeping defect 1 (Magnetic fluid), and defect 2 (hemoglobin) refractive indices constant and changing the refractive index of the defect 3 (urine).

D_{Def}(nm)	Defects3 peak frequency	Q-factor	Concentration(mg/dl)	Refractive Index
1713.6 nm	6.7401 e^{+13}	2339	0–15	1.336
	6.7361 e^{+13}	2217	2.5	1.339
	6.7323 e^{+13}	2090	5	1.342

We apply the above-mentioned analysis to a practical case, by setting the parameters of the photonic sensor to D = 1360 nm such as d_A=952 nm, d_B=408 nm, and d_{Def} = 1713.6 nm. With these sensor settings, the operating wavelength of the device will be close upon the infrared (IR) spectrum. In this spectral domain, the sensor sensibility determined by $S = \Delta\lambda/\Delta n$ is evaluated to be 800 nm/RIU. Figure 6 represents the relationship between the resonant frequency and the refractive index for the three samples filling the cavities, Ferric magnetic fluid (Fig. 6a), Hemoglobin (Fig. 6b), and urine (Fig. 6c) with various concentrations. From the figure, we have a linear relationship between frequency and IR, where the slope represents the sensibility of 800 nm/RIU. A 30.4 Oe change in the concentration of the magnetic fluid, a

0.2 g / l change in the hemoglobin concentration and a 0.015 mg change in the urine concentration may be detectable. The figure of merit, FoM = S / Δλ can also determine the detection performance of photonic structures. The formula of the figure of merit mentions that the narrow resonances improve the detection because they allow a precise determination of the shift of the resonance according to the surrounding medium [30]. The value of the figure of merit FoM of this structure is calculated as 420000 (RIU^{-1}).

Finally, it can be concluded that the proposed sensor exhibits better performance compare to recent published articles. The proposed sensor gains the maximum sensitivity of 800 nm/RIU; FoM of 420000 (RIU^{-1}) and exhibits better outcomes compare to articles [15, 19, 21, 22, 27, 30]. In addition, it can be highlighted that the sensitivity response of proposed model can be enhanced by varying the size of the defect layer in the model. This system could be applied for monitoring in the biomedical sensor for detection of dangerous biological molecules in any magnetic fluid, hemoglobin and/or urine concentration. This work is carried out through the simulation process. In future, we will try to fabricate the model and compare the outcomes with real time results.

4. Conclusion

We have investigated the possibility of using a one-dimensional photonic structure as multichannel sensor. We show that this structure composed by alternating layers of silicon dioxide (SiO_2) and titanium dioxide (TiO_2) can be employed as a highly sensitive sensor to monitor the concentration of three different samples when it is enlightened in normal incidence. We have shown that the width of the defect layer must be correctly adjusted to form a structure allowing to have the three defect modes sufficiently isolated in the transmission spectrum. This sensor offers high sensitivity, 800 nm per refractive index unit (RIU).

Declarations

Acknowledgements: Not applicable.

Authors' contributions: V. D, N. R. R and K. A. developed the idea and supervised the project. A. B., D. B. and H. J. E. contributed to the research of current studies. A. B., S. K., H. J. E. and D. B. were major contributors in writing the manuscript. All authors revised the paper and approved the final manuscript.

Funding: No funding was received for this research.

Availability of data and materials: The datasets used and/or analysed during the current study are available from the corresponding author on reasonable request.

Competing interests: The authors declare that they have no competing interests.

References

1. J. Zhou, Y. Wang, C. Liao, B. Sun, J. He, G. Yin, S. Liu, Z. Li, G. Wang, C. Zhong, J. Zhao, Intensity modulated refractive index sensor based on optical fiber Michelson interferometer, Sens. Actuators B : Chem, 20, 315–3119 (2015).
2. Xiaoling Wang, Zhenfeng Xu, Naiguang Lu, Jun Zhu, Guofan Jin, "Ultracompact refractive index sensor based on microcavity in the sandwiched photonic crystal waveguide structure", *Optics Communications*, vol. 281, no. 6, pp. 1725–1731, 2008
3. Peipeng Xu, Kaiyuan Yao, Jiajiu Zheng, Xiaowei Guan, Yaocheng Shi, "Slotted photonic crystal nanobeam cavity with parabolic modulated width stack for refractive index sensing", *Optics express*, vol. 21, no. 22, pp. 26908–26913, 2013
4. Mehmet A Dündar, Els Cl Ryckebosch, Richard Nötzel, Fouad Karouta, Leo J van IJzendoorn, Rob W van der Heijden, "Sensitivities of ingaasp photonic crystal membrane nanocavities to hole refractive index", *Optics express*, vol. 18, no. 5, pp. 4049–4056, 2010.
5. Y. Zhao, F. Xia, H.F. Hu, C. Du, A ring-core optical fiber sensor with asymmetric LPG for highly sensitive temperature measurement, IEEE T. Instrum. Meas. 66, 3378–3386 (2017).
6. Z. Li, C. Liao, Y. Wang, L. Xu, D. Wang, X. Dong, S. Liu, Q. Wang, K. Yang, J. Zhou, Highly-sensitive gas pressure sensor using twincore fiber based inline Mach-Zehnder interferometer, Opt. Express, 23, 6673–6678 (2015).
7. P. Zubiate, C.R. Zamarreno, I. Del Villar, I.R. Matias, F.J. Arregui, Tunable optical fiber pH sensors based on TE and TM lossy mode resonances (LMRs), Sens. Actuators B: Chem, 231, 484–490 (2016).
8. S. Zhang, M. Ghandehari, J. Ou, Photonic crystal fiber long period grating absorption gas sensor based on a tunable erbium-doped fiber ring laser, Sens. Actuators B: Chem, 223, 324–332 (2016).
9. G.K.B. Costa, M. Paula, M.P. Gouvea, L.M.B. Soares, J.M.B. Pereira, Fernando Favero,Arthur M.B. Braga, P. Palffy-Muhoray, A.C. Bruno, I.C.S. Carvalho, In-fiber Fabry-Perot interferometer for strain and magnetic field sensing, Opt. Express, 24, 14690–14696 (2016).
10. Baraket Z, Zaghdoudi J, Kanzari M Investigation of the 1D symmetrical linear graded superconductor dielectric photonic crystals and its potential applications as an optimized low temperature sensors. Opt Mater 64:147–151(2017)
11. Savarimuthu Robinson, Nagaraj Dhanlaksmi, Photonic Crystal Based Biosensor for the Detection of Glucose Concentration in Urine, Photonic Sensors DOI: 10.1007/s13320016-0347–3 (2016),.
12. John D. Joannopoulos, Photonic Crystals Molding the Flow of Light, Second Edition, Princeton University of press (2008).
13. Yasuhide Tsuji, Photonic Crystal Waveguide Based on 2-D photonic Crystal with Absolute Photonic Band Gap, IEEE Photonic Technology Letters, 18, 15 (2014).
14. Skivesen N. Tetu, M. Kristensen, Photonic crystal waveguide biosensor, Optic Express, 15, 3169–3176 (2007).
15. Bouzidi A, Bria B, Falyouni F, Akjouj A, Lévêque G, Azizi M, Berkhli H A biosensor based on one-dimensional photonic crystal for monitoring blood glycemia. J Mater Environ Sci 8:3892–3896

(2017).

16. J. Wu J, Y. Miao, B. Song, W. Lin, H. Zhang, K. Zhang, B. Liu, J. Yao, Low temperature sensitive intensity-interrogated magnetic field sensor based on modal interference in thin-core fiber and magnetic fluid, Appl. Phys. Lett 104, 252402 (2014).
17. Y.F. Chen, S.Y. Yang, W.S. Tse, H.E. Horng, C.Y. Hong, H.C. Yang, Thermal effect on the field-dependent refractive index of the magnetic fluid film, Appl. Phys. Lett. 82, 3481 (2003).
18. Y. Zhao, Y.N. Zhang, R.Q. Lv, Simultaneous measurement of magnetic field and temperature based on magnetic fluid-infiltrated photonic crystal cavity, IEEE Trans. Instrum. Meas. 64, 1055 (2015).
19. N.R. Ramanujam, Hala J. El-Khozondar, Vigneswaran Dhasarthan, Sofyan A. Taya, Arafa H. Aly, Design of one dimensional defect based photonic crystal by composited superconducting material for biosensing applications, Physica B: Condensed Matter 572, 42–55, 2019.
20. N.R. Ramanujam, I.S. Amiri, Sofyan A. Taya, Saeed Olyaee, R. Udaiyakumar, A. Pasumpon Pandian, K.S. Joseph Wilson, P. Mahalakshmi, P.P. Yuyapin, Enhanced sensitivity of cancer cell using one dimensional nano composite material coated photonic crystal, Microsystem Technologies, 25, Issue 1, pp 189–196, (2019).
21. Hala J. El-Khozondar, P. Mahalakshmi, Rifa J. El-Khozondar, N.R. Ramanujam, I.S. Amirie, P. Yupapine, Design of one dimensional refractive index sensor using ternary photonic crystal waveguide for plasma blood samples applications, Physica E, 111, Pages 29–36 (2019).
22. S. Olyaee, S. Najafgholinezhad, Computational study of a label-free biosensor based on a photonic crystal nanocavity resonator, Applied Optics, 52, 720–7213 (2013).
23. Lucklum R and Li J, **Phononic crystals for liquid sensor applications**, Meas.Sci. Technol. **20 124014 (**2009**)**
24. Bah M L, Akjouj A, El Boudouti E H, Djafari-Rouhani B and Dobrzynski L, Surface and interface optical waves in superlattices: transverse electric localized and resonant modes 1996 J. Phys.: Condens. Matter 8 4171
25. Mir A, Akjouj A, El Boudouti E H, Djafari-Rouhani B and Dobrzynski L, Large omnidirectional band gaps and selective transmission in one-imensional multilayer photonic structures 2001 Vacuum 63 197
26. Bria D, Djafari-Rouhani B, El Boudouti E H, Mir A, Akjouj A and Nougaoui, Omnidirectional optical mirror in a cladded-superlattice structure A 2002 J. Appl. Phys. 91 2569
27. A Bouzidi, D Bria, A Akjouj, Y Pennec and B Djafari-Rouhani, A tiny gas-sensor system based on 1D photonic crystal, J. Phys. D: Appl. Phys. 48 (2015) 495102
28. NoamaOuchani, AbdelazizElMoussaouy, HassanAynaou, YoussefElHassouani, El HoussaineElBoudouti, BahramDjafari-Rouhani, Optical transmission properties of an anisotropic defect cavity in one-dimensional photonic crystal (2015).
29. Wiechmann S, Müller J (2009) Thermo-optic properties of TiO2, Ta2O5 and Al2O3 thin films for integrated optics on silicon. Thin Solid Films 517:6847

30. Afaf Bouzidi, Driss Bria, Abdellatif Akjouj, **Hayat Berkhli, Optical liquid sensor based on periodic multilayers structure (**2016**)**.

Figures

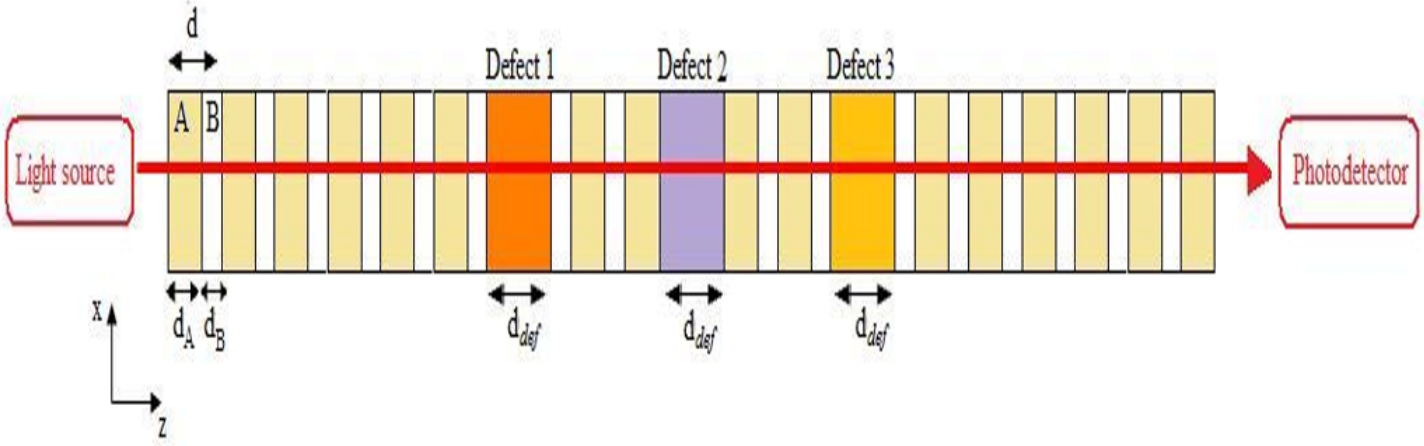

Figure 2

Representation of the sensor allowing the simultaneous detection of the concentration of three analytes, where layer A and layer B, respectively represent the layers of silicon dioxide (SiO2) and titanium dioxide (TiO2), and the defect represents the analytes to be detected.

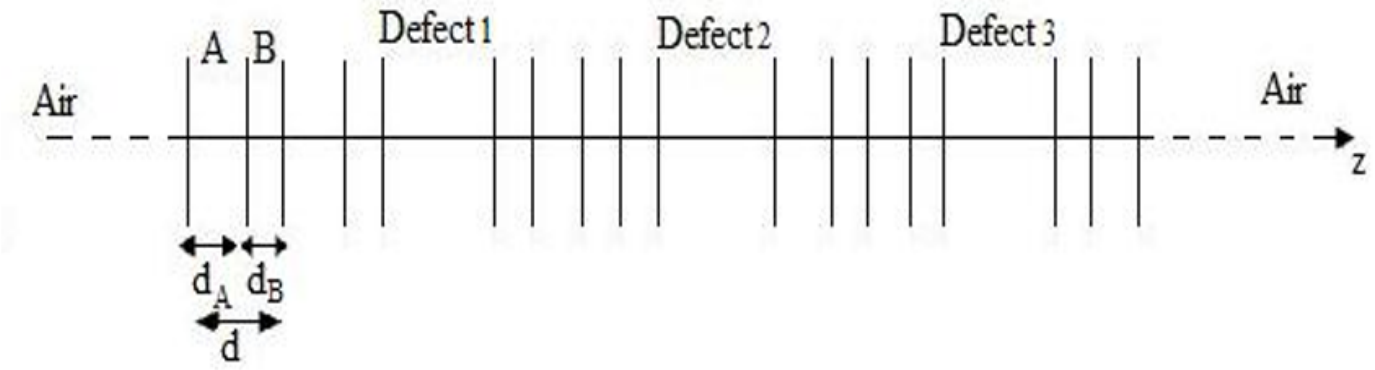

Figure 4

Structure of the calculation. A and B represent, respectively, the layers of silicon dioxide (SiO2) and of titanium dioxide (TiO2) and the defect represents the analytes to be detected.

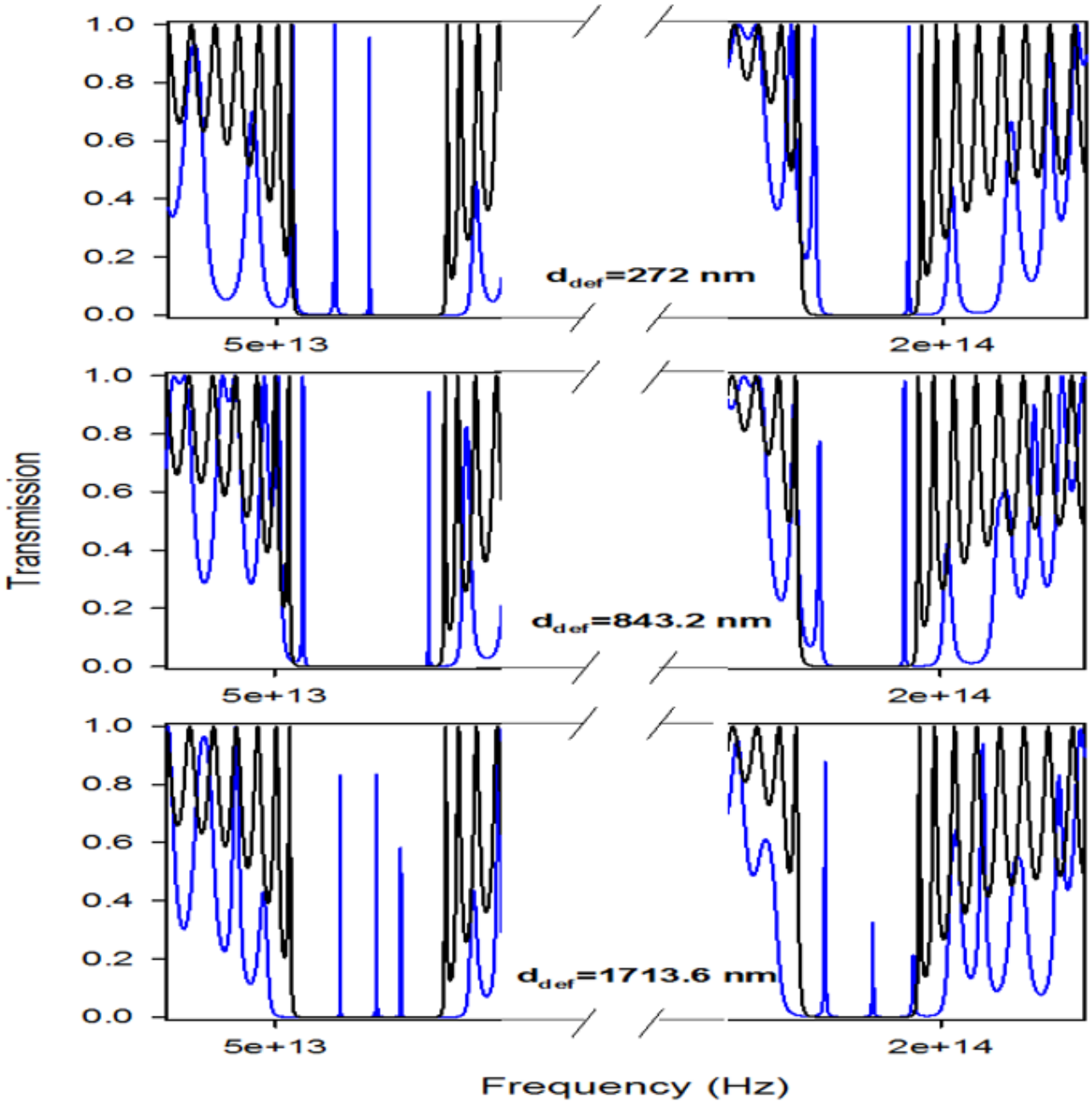

Figure 6

Transmission curves of the crystal shown in Fig. 1 with the first cavity filled by the magnetic fluid (89.9Oe of concentration), the second cavity filled with Hemoglobin (10g / l of concentration), and the third cavity filled with urine (15 mg / dl of concentration) for dDef = 272 nm (a), dDef = 843.2 nm (b) and dDef = 1713.6 (c) at normal incidence.

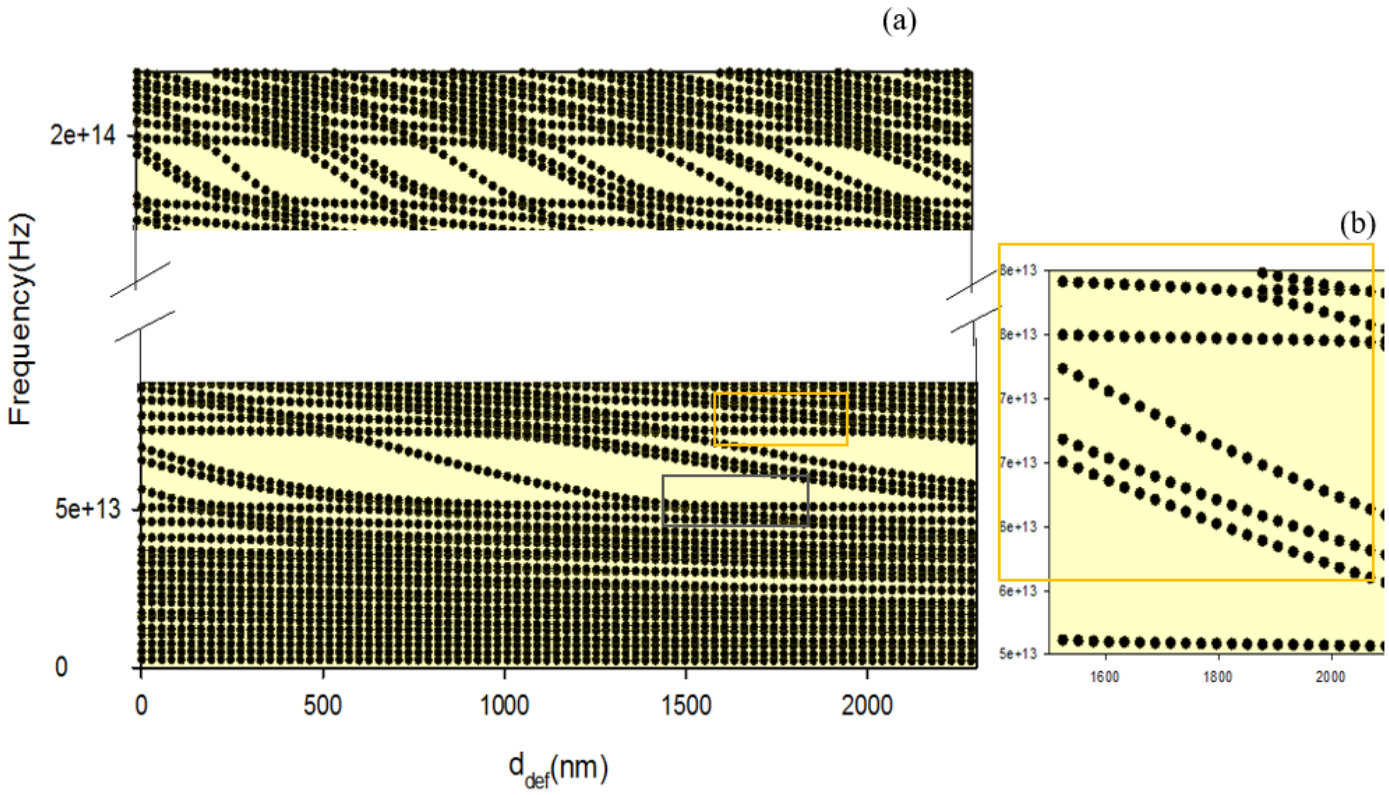

Figure 8

Transmission frequency versus dDef for the structure of Fig. 2 when the cavities are filled with samples (a), a zoom on the boxed area (b).

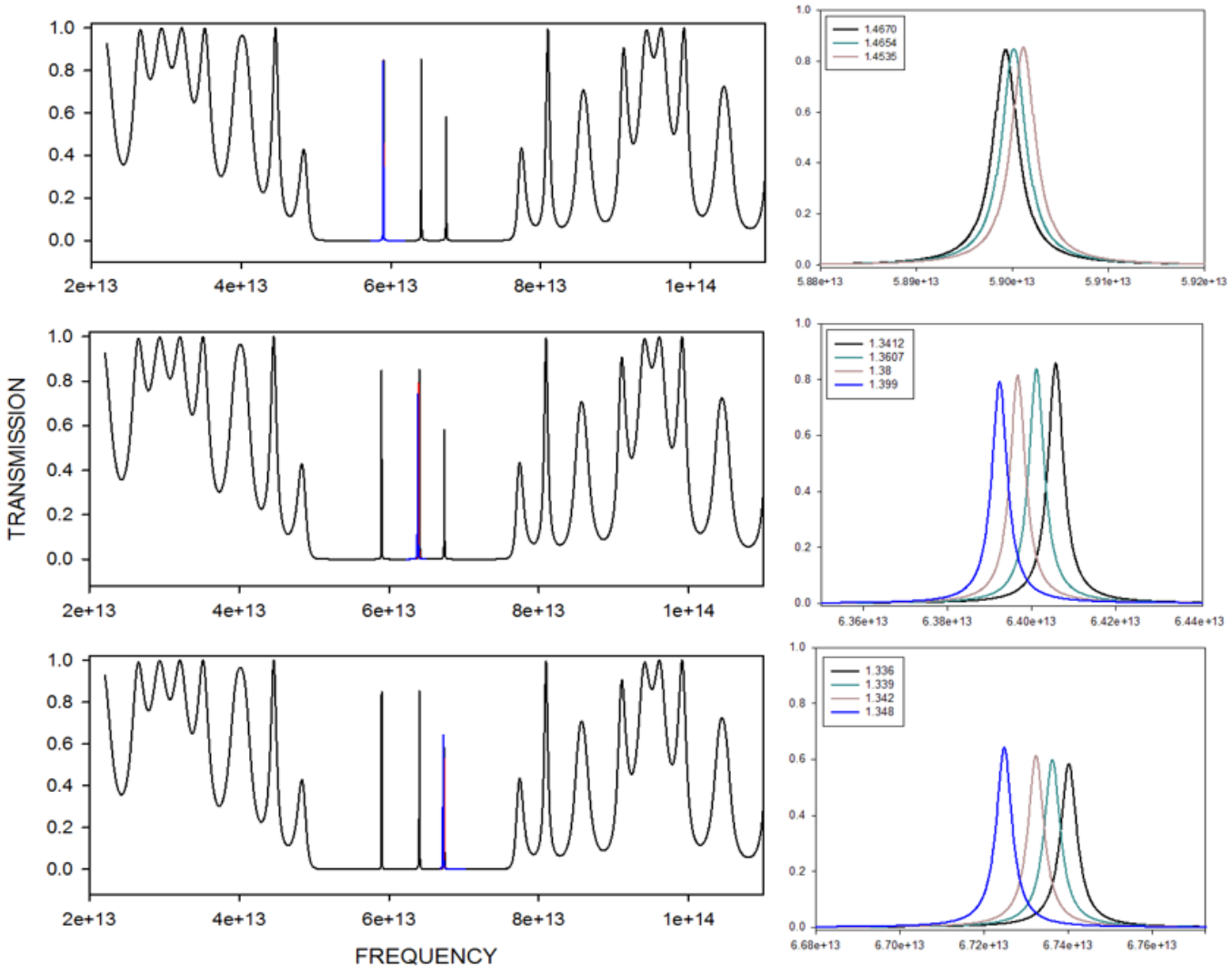

Figure 10

Transmission spectra with different refractive indices for each sample.

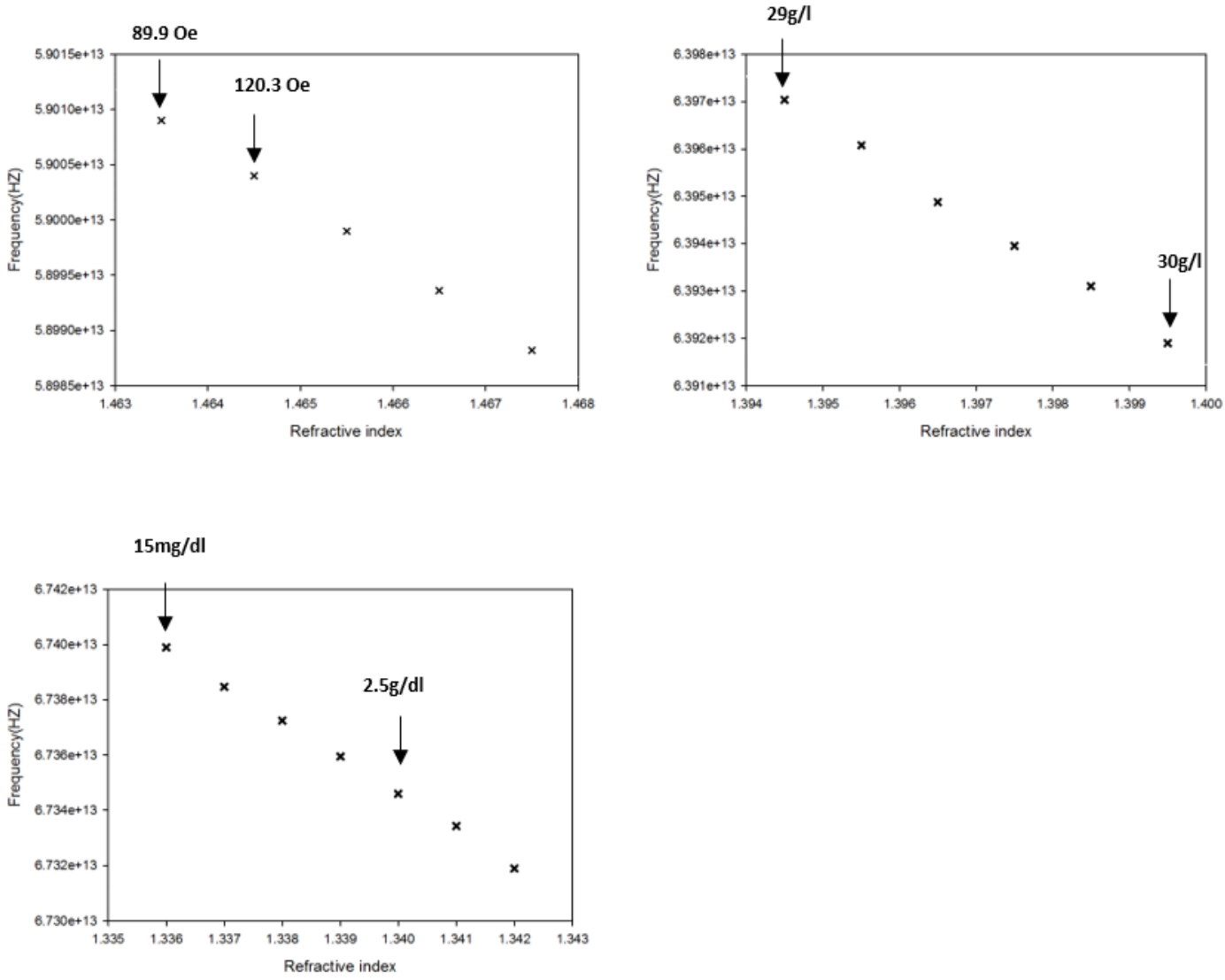

Figure 11

Frequency as a function of the concentration of the sample highlighting two concentrations of Ferric magnetic fluid in the first cavity (a), Hemoglobin in the second cavity (b), urine in the third cavity (c)